Research Article

Journal of Environmental Nanotechnology

Fabrication and Characterization of Bio-hybrid Composites Reinforced with *Sansevieria cylindrica,* Bamboo Fibers, Areca Sheath Powder, and ZnO Nanoparticles

N. Devendran* and T. S. Lakshmi

Department of Civil Engineering, Saveetha School of Engineering, Saveetha Institute of Medical and Technical Sciences, Chennai, TN, India

Received: 29.08.2025 Accepted: 20.09.2025 Published: 30.09.2025

*nmdev24@gmail.com

ABSTRACT

This study reports the fabrication of advanced hybrid composites using compression molding and hand layup techniques. The composites incorporated 1–3 wt% areca sheath powder and ZnO nanoparticles with 20 wt% *Sansevieria cylindrica* and bamboo fibers as reinforcements. Their properties were evaluated through tensile, impact, dynamic mechanical, vibration, and flammability testing. Results showed significant improvements, achieving a tensile strength of 133.11 MPa and a modulus of 15.07 GPa for one of the samples. Dynamic mechanical analysis revealed superior viscoelastic properties with a storage modulus of 2220 MPa and a loss modulus of 120 MPa. Fire-retardant performance was enhanced, with a reduced heat release rate of 104.05 kW/m^2 and total heat release of 183.39 MJ/m^2. Vibration analysis indicated improved structural stability with a natural frequency of 101 Hz. These findings highlight the potential of the developed hybrid composites for high-performance applications in aerospace, automotive, marine, construction, and infrastructure sectors.

Keywords: Hybrid composites; *Sansevieria cylindrica* fiber; Dynamic mechanical analysis; ZnO nanoparticles.

1. INTRODUCTION

Natural fiber-reinforced composites (NFRCs) have garnered significant interest across several industries due to their recyclable properties, which contribute to the development of eco-friendly products. *Sansevieria cylindrica* (SC) fiber-reinforced natural rubber composites were fabricated by compression molding (Palanisamy *et al.* 2023). *Sansevieria cylindrica* fiber composites were prepared with treated and untreated fibers at varying weight percentages. Treated fibers showed stronger interfacial bonding and superior performance than untreated ones (Subramaniam *et al.* 2022). Poly lactic acid/bamboo filler composites (50:50 and 60:40) were produced without fiber pretreatment. Infra-red spectroscopy showed composition-dependent functional changes, but stiffness and wear resistance did not improve (Sasaki *et al*. 2024). Immersing the *Enset ventricosum* fibers in a 4 wt% NaOH solution for 4 hours at ambient temperature enhanced their interfacial adhesion with polymer matrices (Ponnuswamy *et al*. 2024). *Bambusa tulda* fiber reinforced cashew nut shell polymer composites were developed with NaOH treatments (2–10%). The best properties were observed at 6% NaOH, achieving a tensile strength of 132.91 MPa, a storage modulus of 8378 MPa, and a crystallinity index of 51.73% (Saha *et al.* 2024).

Poly lactic acid composites with bamboo charcoal and chitosan showed improved flame retardancy and strength. Flammability tests confirmed reduced peak heat release rate (pHRR) (−26.9%) and total heat release (THR) (−30.5%) due to stable char formation (Li *et al.* 2021). Prosthetic composites using sea urchin chitin, basalt-encapsulated bamboo fiber, and epoxy were developed and showed superior thermal conductivity (0.72 W/mK), and low flame spread (5.72 mm/min) (Khan *et al.* 2024). Lightweight prosthetic composites were fabricated with silane-treated polyethylene terephthalate foam and areca fiber reinforced in vinyl ester. Silane treatment improved interlaminar shear strength, resistance to delamination, and maintained fire-retardant and thermal properties under accelerated aging (Khan *et al.* 2024b).

Bamboo fiber reinforced high density polyethylene composites were modified with boric acid–borax (Ba-Bx) pretreatment, ammonium polyphosphate (APP), and nano-SiO_2. The best flame resistance was achieved at Ba-Bx 5%/APP 15%, with the highest limiting oxygen index (LOI) 13%/nano- SiO_2 2%. (Kumar and Chauhan, 2022). Wood–plastic composites with bamboo fibers (alkali/Boric acid-Borax treated) and APP were developed. APP 10%/Ba-Bx 5% reduced heat release rate (HRR) by 69%, pHRR by 59%, THR by

48%, and increased ignition time by 62% (Kumar *et al.* 2022). Snake Grass Fiber/epoxy composites with coconut shell ash (CSA) filler (2.5–10 wt%) were fabricated. Thermogravimetric analysis (TGA) showed maximum char yield (16.56%) at 10 wt% CSA, with enhanced biodegradability but reduced thermal conductivity (Iyyadurai *et al.* 2023).

Hybrid composites with African teff and SCF (5–25 wt%) and castor seed shell powder filler were prepared. Fibers were alkali-treated to enhance adhesion, confirmed by FTIR and SEM (Manickaraj *et al.* 2022). Hybrid composites using jute, SGF, kenaf, and custard apple seed powder (CASP) were fabricated. The best composition (sample C: 5% JF, 8.75% SGF+KF, 7.5% CASP, 70% epoxy) showed tensile strength 60.43 MPa and compressive strength 48.31 MPa (Ramadoss *et al.* 2024). Wood dust/epoxy composites with ZnO nanoparticles (0.1–1 vol.%) were fabricated by casting. Flexural strength and hardness improved up to 0.5 vol.% ZnO, then decreased due to agglomeration. SEM confirmed uniform dispersion at low filler content (Al-Lhaibi *et al.* 2022). *Ceiba petandra* fiber/polyester composites were reinforced with snail powder (SP). Increasing SP improved tensile strength, density, char yield, LOI, and thermal resistance. Flammability rate decreased since SP inhibited oxygen and gas diffusion. Dynamic mechanical analyzer and TGA confirmed better thermal stability with higher SP filler (Diharjo *et al.* 2024).

Aramid fiber/epoxy composites modified with 5 wt% multifunctional flame-retardant achieved LOI of 37.5%, self-extinguishing ability, and reduced heat/smoke release. Good compatibility ensured both flame retardancy and toughness without compromising thermal stability (Lan *et al.* 2024). Flax–basalt/epoxy laminates with ZnO nanofillers were fabricated by hand layup. Higher basalt content composites showed superior tensile (79 MPa), flexural (81 MPa), impact (23 J), thermal conductivity (0.199 W/mK), and heat deflection temperature (87 °C). ZnO addition improved thermal properties by ~4% (Raja *et al.* 2024). Bamboo fiber eco-composites with eggshell powder and cardboard waste were developed by compression molding. A-type (30% bamboo) showed the lowest thermal conductivity (58.20 mW/mK), achieving 310% higher insulation than the virgin matrix (Velmurugan *et al.* 2025).

Henequen fiber/epoxy composites reinforced with CuO nanoparticles were fabricated. The composite with 15 g CuO exhibited the highest tensile (76.19 MPa), flexural (81.29 MPa), impact (17.92 kJ/m^2), and hardness (67 Shore D). TGA revealed improved thermal stability (20% char yield at 500 °C) (Raja *et al.*2025). Hemp/PP composites were reinforced with ZnO and SiO_2 microparticles (2–8 wt.%) by vacuum backing. The 4 wt.% SD + ZO composite showed an increase in tensile strength (+10.36%) and flexural strength (+3.21%) due to improved stress transfer at the interface. The thermal conductivity was 0.0583 W/mK, lower than 0.065 W/mK, confirming retained insulation with enhanced flame resistance (Velmurugan *et al.* 2023).

Although natural fiber composites such as *Sansevieria cylindrica* and bamboo have been individually studied for their mechanical and thermal behavior, very limited work has examined their role in reducing vibration and enhancing fire resistance, which are crucial for structural and automotive applications. Existing studies on fillers like ZnO nanoparticles and areca sheath powder primarily emphasize improvements in strength or dynamic mechanical properties, but their combined effect on free vibrational attributes (natural frequency, damping) and fire-retardant characteristics (heat release rate, smoke release, ignition resistance) has not been systematically addressed. The novelty of this study lies in developing hybrid epoxy composites reinforced with *Sansevieria* and bamboo fibers, modified with ZnO nanoparticles and areca sheath powder, and evaluating them across mechanical, dynamic mechanical, vibrational, and fire-retardant performance. This dual-filler approach introduces a synergistic effect, where ZnO enhances stiffness and interfacial bonding while areca sheath powder improves thermal stability and flame resistance, thereby bridging the research gap and expanding the potential of natural fiber composites for engineering applications requiring both vibration damping and fire safety.

2. MATERIALS AND METHODOLOGY

2.1 Materials

This research focuses on composite materials that enhance mechanical properties by integrating natural fibers with various fillers. This research utilizes reinforcements, matrix materials, and fillers obtained from several sources in Tamil Nadu, India. The reinforcements *Sansevieria cylindrica* fiber, (density 0.72 g/cm^3) and bamboo fiber (density 0.9 g/ cm^3), both provided in 250 GSM were procured from Gogreen Enterprises, Chennai. The matrix materials consist of epoxy resin (LY556) with a density of 1.2 g/ cm^3 and its associated hardening agent (HY951) with a density of 1.1 g/cm^3, obtained from Kovai Cheenu Enterprises, Coimbatore. The incorporated fillers comprise areca sheath powder collected locally from diverse locations in Coimbatore. ZnO nanoparticles, characterized by a density of 5.61 g/cm^3 and an average particle size of 40 nm, were procured from Matrics Enterprises, Nagercoil, Tamil Nadu, India.

The naturally shed areca nut sheaths were gathered and thoroughly washed with distilled water to remove dust, pollutants, and microbiological contaminants before ground into powder form. The sheaths were oven-dried at a regulated temperature (often 60-80 °C) to eliminate residual moisture until a stable

weight was attained. The dried sheaths were initially cut into small fragments and subsequently processed in a ball mill to produce a fine powder (Singh *et al.* 2020). To maintain uniformity in particle size for future applications, the powder was sieved through a standard mesh with a size range 100-200 µm. The areca sheath powder was stored in airtight containers to prevent microbial growth and moisture absorption.

2.2 *Sansevieria cylindrica* and Bamboo Fibres

Composites derived from *Sansevieria cylindrica* have superior load-bearing capacity and uniform dimensions due to the plant's high cellulose content, rigidity, and exceptional tensile strength. Bamboo fiber enhances vibration-damping properties while also being remarkably strong, flexible, and thermally stable (Ngouobe *et al.* 2024). These fibers synergistically enhance mechanical and thermal properties for green composite manufacture while being environmentally sustainable.

2.3 Areca Sheath Powder

Areca sheath powder was selected as a biofiller due to its biodegradability, low density, and lignocellulosic composition. The composite's mechanical performance is enhanced by lignin, cellulose, and hemicellulose, which promote interfacial adhesion with polymer matrices. The natural filler enhances material strength, reduces density, improves eco-sustainability, and lowers overall material costs. This is a sustainable, reinforcing alternative for green composite fabrication, owing to its organic composition, which enhances biodegradability and environmental compatibility.

2.4 ZnO Nanoparticles

The incorporation of zinc oxide nanoparticles as a filler material improved the mechanical, thermal, and functional properties of the composite (Sathish Kumar *et al.* 2023). The incorporation of ZnO into the polymer matrix enhances its strength and stiffness, rendering it more resistant to wear and scratches, even under dynamic loading conditions. The antibacterial and UV-protective properties of ZnO enhance the composite's durability and functionality. It is a beneficial additive for advanced structural and protective applications because of its ability to improve thermal stability and reduce degradation at elevated temperatures.

2.5 NaOH Treatment of Natural Fibres

The natural fibers, comprising *Sansevieria cylindrica* and bamboo, were initially submerged in clean water at ambient temperature to remove any surface impurities, waxes, or dust. Subsequently, they were allowed to desiccate for 48 hours in a controlled setting. Before the chemical modification, this pretreatment ensured the elimination of all contaminants. Subsequent to drying, the fibers underwent treatment with an alkali solution comprising 4wt% NaOH for a duration of 4 hours at ambient temperature. This mercerization process aimed to enhance interfacial adhesion with the polymer matrix and augment fiber roughness by dissolving amorphous constituents, including hemicellulose, lignin, and pectin. Subsequent to the treatment, the fibers were subjected to numerous rinses with deionized water until the effluent attained a neutral pH. This guaranteed the thorough removal of any residual alkali. Subsequent to drying to eliminate excess moisture, the fibers were encased in plastic bags to inhibit air circulation. The next phase in their preparation for composite manufacture was storing them in a dry container under a controlled atmosphere, maintaining a relative humidity of approximately 40%.

Table 1. Weight proportions in the proposed composites

Sample	Matrix Proportion (wt%)	Reinforcements (wt%)	Areca Sheath Powder (wt%)	ZnO Nanoparticles (wt%)
S1	100	0	0	0
S2	80	20	0	0
S3	79	20	0	1
S4	78	20	0	2
S5	79	20	1	0
S6	78	20	2	0
S7	78	20	1	1

2.6 Preparations of Composites

The composite was fabricated using a hand layup technique and compression molding. To ensure uniform distribution after molding and testing, the ratio of 80% varying matrix material to 20wt% reinforcement was confirmed at this stage of the composite production process, with a ratio of 1:1 *Sansevieria cylindrica* and bamboo fiber. Fillers, including areca sheath powders and ZnO nanoparticles, constituted 1% to 2% by weight in relation to the matrix. This experiment attained superior filler dispersions within the matrix by gradually incorporating these fillers into epoxy resin LY556 before the addition of hardener HY951. To prevent material aggregation and ensure uniform distribution of nanoparticles and powders, the mixture was mechanically agitated at 300 rpm (Gupta *et al.* 2024). Table 1 shows seven distinct plate composites, fabricated with filler concentrations varying from minimal to maximal.

The hardener was combined with the epoxy resin in a 10:1 ratio to guarantee adequate curing and consistent adhesion. The hybrid composite was constructed with four separate layers organized in the sequence SBSB: *Sansevieria cylindrica*, bamboo fiber, *Sansevieria cylindrica*, and bamboo fiber. A layer of *Sansevieria cylindrica* was initially used as the outermost reinforcement to efficiently endure compressive and tensile loads. A layer of bamboo fiber was subsequently added, serving as a core support to augment the load-bearing capability of the composite. The third layer comprised *Sansevieria cylindrica*, enhancing structural integrity and mitigating crack propagation. The core bamboo layer enhanced impact resistance and facilitated a balance of strength and flexibility across the laminate. After the fibers were successively arranged, the resin–hardener mixture was consistently administered, guaranteeing thorough impregnation of each layer. Steel rollers were utilized to remove trapped air bubbles and to enhance the intimate interaction between fibers and the resin matrix. The selected SBSB design optimized stress distribution, resulting in improved tensile, flexural, and impact capabilities, with bamboo layers aiding the *Sansevieria cylindrica* reinforcements in preserving dimensional stability and mechanical efficiency. The completed hand layup application resulted in the formation of a closed mold, which was subsequently heated at 120 °C for 120 minutes. Upon completion of compression molding, the mold was allowed to cool to ambient temperature for a duration of approximately 120 minutes (Giridharan *et al.* 2024). The process provided hybrid laminates measuring 270 mm × 210 mm × 3 mm, incorporating areca sheath powder, ZnO nanoparticles, and fibers from *Sansevieria cylindrica* and bamboo fibers.

2.7 Mechanical Testing

Subsequent to sample preparation, the composite plates were sectioned utilizing a circular saw fitted with tungsten carbide discs, as per the requirements delineated in Fig. 1. The cutting technique was executed in compliance with the specifications outlined in ASTM D6110 for impact testing, ASTM D790 for flexural tests, and ASTM D3039 for tensile tests (Krishnasamy *et al.* 2025). The tensile samples measure 250 × 25 × 3mm in thickness. The tensile test was conducted at room temperature with a crosshead speed of 2 mm/min using a universal tester equipped with a 100 kN load cell. The true strain was computed using a clip-gauge extensometer. The flexural tests were performed using the same configuration, with a crosshead speed of 2 mm/min and a 1 kN load cell. In each case, five samples were analyzed.

2.8 Dynamic Mechanical Analysis

The dynamic mechanical properties of the specimens were evaluated according to ASTM D 5023, utilizing dimensions of 50 × 13 × 3 mm^3. The current analysis employed the processing parameters: temperature range 10-100 °C, frequency of 5 Hz, and a heating rate of 12 °C min^{-1}, conducted using the dynamic mechanical analyzer (TA Instruments DMA Q800).



Fig. 1: Universal testing machine specimen of (a) tensile, (b) flexural and (c) impact test

2.9 Flammability Testing

Flammability was assessed using a cone calorimeter with ISO 5660. A 50 kW/m^2 heat flux was applied externally. The dimensions of the sample were 100 × 100 × 3 mm. The specimens were arranged horizontally, with an edge frame utilized for each test.

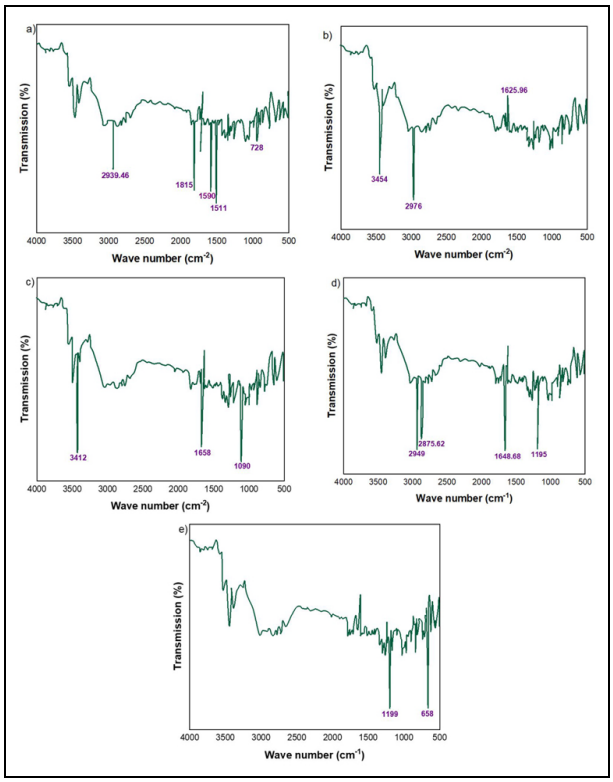


Fig. 2: FTIR characterization of hybrid composites: (a) S3, (b) S4, (c) S5, (d) S6 and (e) S7

2.10 Vibration Analysis

Vibration analysis was done using an impact hammer instrument. This device had a robust impact sledgehammer. Subsequently, accelerometers were

affixed to the sample. The specimen was shaped rectangularly with dimensions of 20 × 2 × 0.3 cm^3. The composite samples were struck three times by the impact hammer at regular intervals. The accelerometer's response signal was documented utilizing a data acquisition system. The signals generated by striking the material were captured using two distinct adapters: one connected to the hammer and the other to the accelerometer.

2.11 FTIR and Morphological Analysis

FTIR spectrometer (BRUKER, Germany) was utilized to confirm the chemical functionalities and binding properties of hybrid materials, including *Sansevieria cylindrica*/Bamboo-reinforced ZnO nanoparticles and areca sheath powder. Employing attenuated total reflection, the range of detection extended from 4000 to 500 cm^{-1}. A scanning electron microscope (SEM) was employed to examine the fractured tensile specimen of the composite materials composed of Bamboo/*Sansevieria cylindrica* fibers, ZnO nanoparticles, and areca sheath powder to investigate their morphological characteristics. SEM revealed enhanced fiber–matrix bonding, reduced delamination, and stronger failure morphology (Harak *et al.* 2024).

3. RESULTS AND DISCUSSIONS

3.1 FTIR Analysis

Fig. 2 illustrates that samples S3 and S4 exhibited peaks at 2939 cm^{-1} (-CH Stretch), 1815 cm^{-1} (carbonyl), 1590 cm^{-1} (lignin), 728 cm^{-1} (-COOH) and 1511 cm^{-1} (-CH_2). Subsequently, peaks were seen at 3432, 2939, and 1815–1590 cm^{-1}, respectively, indicating the presence of the SiO_2 functional groups. The peak at 2939 cm^{-1} corresponds to the stretching vibration of C-H bonds in organic compounds, such as polymers or natural fibers. This indicates the presence of hydrocarbon chains or organic molecules. Compounds containing carbonyl groups, such as ketones, aldehydes, esters, and carboxylic acids, are typically identified by C=O stretching vibrations, evidenced by the carbonyl signal at 1815 cm^{-1}. A peak at 1590 cm^{-1} corresponding to an aromatic C=C stretching vibration signifies the presence of lignin, a complex organic polymer located in plant cell walls. The findings indicate the existence of lignin-derived components in the sample. The signal at 728 cm^{-1} results from the bending vibration of carboxylic acid (-COOH) groups. This indicates that the sample comprises organic acids, potentially associated with materials derived from biomass. The vibrations at 1511 cm^{-1} correspond to the bending of the -CH_2 bond. FTIR confirmed chemical bonding improvements (Prabhu *et al.* 2022).

FTIR revealed that samples S5 and S6 exhibited 3412 cm^{-1} (O-H), 1658 cm^{-1} (H-O-H), 1090 cm^{-1} (Si-O), and 1121 cm^{-1} (S-O-Si). The peak at 3412 cm^{-1} corresponds to the stretching vibrations of the hydroxyl groups. In materials that often contain hydroxyl groups or water, indicative of hydration or moisture, the bending vibrations of water molecules are represented by the peak at 1648 cm^{-1} (H-O-H). The molecule possesses a sulfur-oxygen-silicon linkage, indicated by the signal at 1121 cm^{-1} (S-O-Si). This may indicate the presence of sulfur-containing compounds or sulfates in the sample. The peaks between 1200 and 800 cm^{-1} are indicative of polymorph cristobalite.

The specimen S7, comprising ZnO nanoparticles and areca sheath powder, demonstrates that the asymmetric stretching vibration of Si-O-Si approximately between 1100-1200 cm^{-1}. The peak at about 1180 cm^{-1} is associated with Si-O stretching vibrations. Areca sheath powder predominantly consists of dolomite, olivine, feldspar, and plagioclase. The FTIR spectra of these minerals exhibit distinct peaks, which correlate directly with their features. The Si-O stretching vibrations in plagioclase feldspar manifest as peaks within the 1000 to 1200 cm^{-1} range.

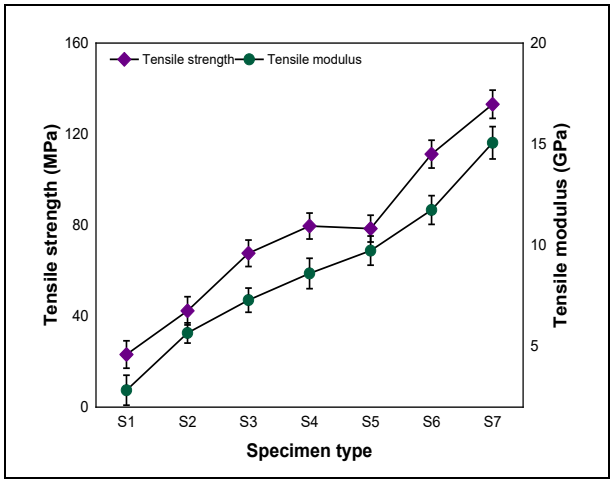


Fig. 3: Tensile strength and modulus of bamboo/*Sansevieria cylindrica*/areca sheath powder/ZnO-based hybrid composites

The existence of hydroxyl groups, silicon-oxygen bonds, and zinc-based compounds is evidenced by OH stretching vibrations 3412 cm^{-1}, Si-O bonds 1090 cm^{-1}, and peaks corresponding to cristobalite and zinc within the range of 1200-1000 cm^{-1}, observed in S5 and S6. The key confirmation of ZnO/areca sheath–matrix interactions comes from (i) the enhanced –OH stretching (3412–3432 cm^{-1}) and COOH bending (728–658 cm^{-1}), (ii) shifts in C=O and aromatic lignin peaks (~1815, 1590 cm^{-1}), and (iii) the emergence of Zn–O–Si/Si–O–Si vibrations (1121–1180 cm^{-1}). These spectral changes verify chemical bonding, hydrogen bonding, and interfacial coordination between fillers and the epoxy matrix, directly contributing to the observed improvements in tensile, flexural, and impact properties.

Samples S3 and S4 exhibit peaks indicative of organic compounds, lignin, and carboxylic acid groups, implying the potential integration of constituents derived from biomass. These ZnO-based coatings further substantiate the reported mechanical improvements. The bands in FTIR indicate the mineral compositions of areca sheath powder and the Si-O-Si asymmetric stretching vibrations of the ZnO component, both of which enhance the composite's strength. Composites containing these functional groups and materials exhibit enhanced interfacial adhesion and increased stiffness, rendering them more resistant to deformation and fracture propagation.

3.2 Mechanical Properties

3.2.1 Tensile Properties

Fig. 3 illustrates the tensile strength and modulus of hybrid composites composed of bamboo fiber, *Sansevieria cylindrica*, areca sheath powder, and ZnO nanoparticles. A significant enhancement in tensile values was observed with the addition of reinforcements or fillers. An exemplary demonstration of how reinforcements might enhance mechanical performance is presented by S1, which exhibited a low tensile strength of 23.13 MPa and was composed completely of epoxy resin. The incorporation of initial reinforcements into S2 resulted in a tensile strength of 42.33 MPa, which was marginally superior to that of S1. Nonetheless, the performance of S2 was lower compared to other samples. Fiber pullout is probably the cause, particularly in unreinforced and filler-free composites.

The bonding between matrix and fiber was inadequate, resulting in ineffective diminished TS and load transmission, as evidenced by this fiber pullout. Inadequate bonding induces the formation of stress-sensitive regions inside the composite. Conversely, S3, which incorporated ZnO nanoparticles, exhibited reduced fiber pullout, indicating enhanced adhesion between the surfaces. The improved load transfer among the fiber and the matrix, facilitated by the ZnO fillers, resulted in superior bonding and increased tensile strength observed in S3.

The tensile strength of the *Sansevieria cylindrica*/Bamboo fiber mat exhibited a consistent increase from S3 to S7, a maximum of 78.45 MPa at S5, with 20% reinforcements and 1% areca sheath powder. S7, comprising 78% matrix material, 20% reinforcements, 1% areca sheath powder, and 1% ZnO nanoparticles, exhibited the highest tensile strength of 133.11 MPa, attributable to the incorporation of fillers that further enhanced its tensile properties. As the fiber content of the composites increased to an optimal 20 wt%, it became progressively more challenging to fracture the specimens, as they could endure greater loads. The interfacial bonding or debonding between fibers and the matrix mostly accounts for the enhanced tensile strength. Interfacial bonding qualities, essential for enhancing composites and dependent on the nature of the interfaces formed, are also examined. Similarly, neem gum powder and snake grass fibre reinforced epoxy composites were studied with varying fiber content (5–35%). The best combination was 30% SGF + 15% neem gum + 55% epoxy, yielding tensile strength 36.49 MPa and flexural strength 65.87 MPa. Higher fiber loading reduced adhesion, but composites showed potential for automotive and aerospace interiors (Pachiappan *et al.* 2023). The improved composite properties result from the robust adhesion between the matrix and the fibers, facilitating effective stress transfer. The previously reported results are corroborated by Fig. 4a and 4b.

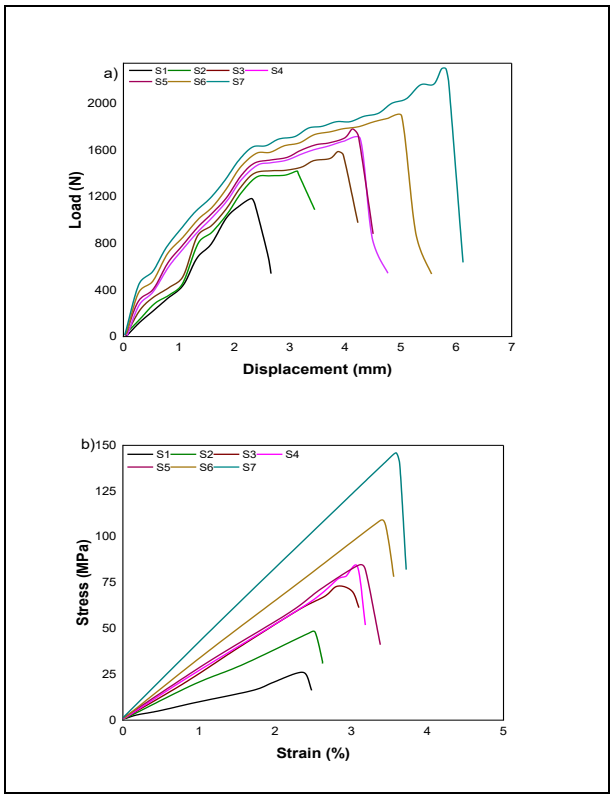


Fig. 4: Tensile behaviour of hybrid composites: (a) stress–strain curves and (b) load–displacement curves

The tensile properties are significantly enhanced by the addition of filler materials. This enhancement increases modulus and tensile strength of composites by rendering the matrix stiffer and establishing an additional barrier to fracture propagation. A balance between components of a composite is essential to enhance its mechanical properties. Similar to other composites, S7 demonstrates a significant influence of fillers and reinforcement. These results align with the conventional perspective in materials science that the composition and selection of materials significantly influence the enhancement of mechanical properties across many engineering applications. In a reported work, biolaminates of ixtle and henequen fibers

reinforced bio-epoxy with ZnO (1–3 wt.%) were produced by vacuum infusion. Ixtle laminates weakened with higher ZnO, while henequen showed the best strength at 2 wt.% ZnO. ZnO altered interlaminar adhesion, affecting fracture behavior differently in both fibers (Torres *et al.* 2022). In the present work, the fibers exhibit a high load-bearing rupture prior to the matrix, as illustrated in SEM image. This results in the increased tensile strength observed in sample S7. The composite is enhanced and rigidified by uniformly distributed reinforcing materials and fillers, which facilitate load transmission and stress distribution.

3.2.2 Flexural Properties

Fig. 5 shows the flexural strength and modulus of the composites. The flexural strength measurements indicate a positive correlation with the addition of fillers and reinforcements to composite materials. The sample containing only epoxy resin exhibits a flexural strength of 47.22 MPa. This value underscores the necessity for superior reinforcing agents to improve the resistance of materials to bending pressures.

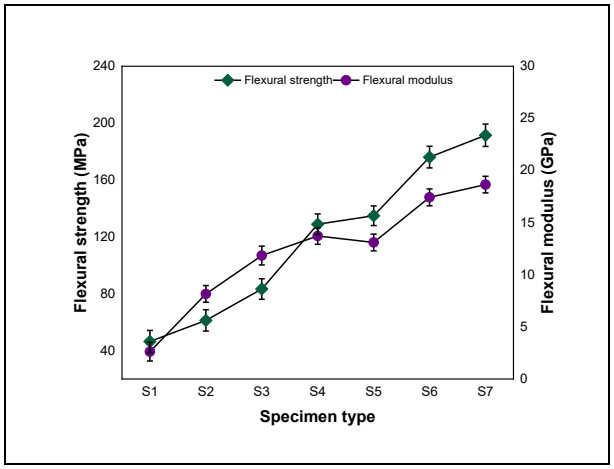


Fig. 5: Flexural strength and modulus of bamboo/*Sansevieria cylindrica*/areca sheath powder/ZnO-based hybrid composites

Flexural strength rises linearly with the percentage of *Sansevieria cylindrica*/Bamboo fiber mat, commencing at S2 and advancing to S5. Sample S5 comprising 20% reinforcements and 1% areca sheath powder, attains a maximum flexural strength of 128.22 MPa. This increase is feasible due to the ability of natural fibers to evenly distribute stress within the matrix and their resistance to bending forces. To improve the stiffness, crack resistance, and flexural strength of the matrix, ZnO nanoparticles and areca sheath powder were employed as fillers. Fig. 6a and 6b illustrate the flexural test result of load-displacement and stress-strain curves.

Compared to all the samples, S7 exhibits the highest flexural strength at 192.97 MPa. The composition consists of 78% matrix, 20% reinforcements (*Sansevieria cylindrica*/Bamboo fiber mat), 1% areca sheath powder, and 1% ZnO nanoparticles. The integration of these components enhances the flexural properties of this composition, resulting in superior attributes. S7 is an ideal selection for high-integrity constructions requiring resistance to deformation due to its superior bending strength. The influence of reinforcement and filler materials on flexural strength and modulus is evidenced by an average enhancement of over 312.9% in flexural strength relative to S1. Similarly, Silane-treated coconut shell powder, areca nut powder, and corn husk fiber in epoxy (hand layup) showed optimum strength (tensile 88.88 MPa, flexural 175.89 MPa, impact 5.3 J, hardness 85.8 Shore-D) (Narayanan *et al.* 2024). Moreover, the apparent improvement is intensified in flexural scenarios due to the material's distinctive stress distribution characteristics when subjected to bending.

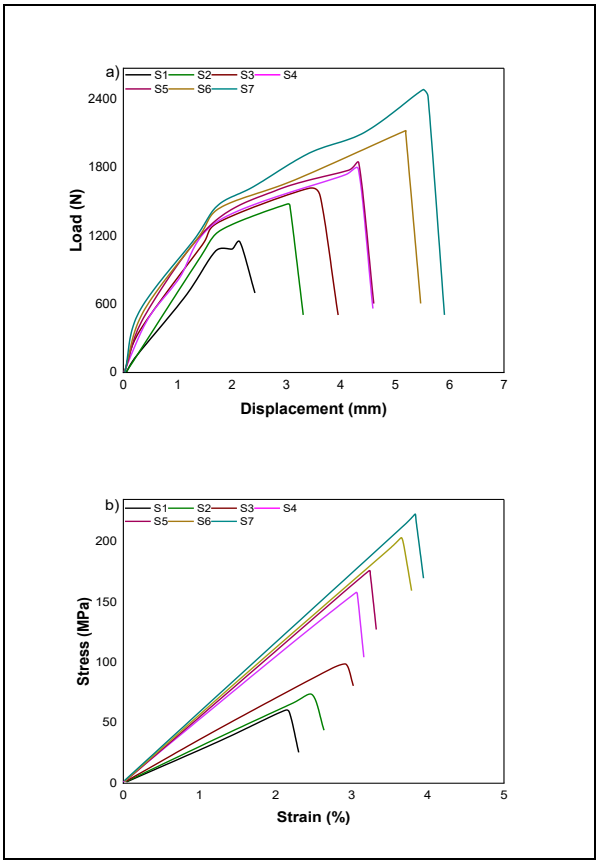


Fig. 6: Flexural test results of hybrid composites: (a) load–displacement curves and (b) stress–strain curves

3.2.3 Impact Properties

The impact strength of the composites is illustrated in Fig. 7. The incorporation of reinforcements and fillers into the composites markedly enhances their impact strength, as indicated by the results. The impact strength test of 2.12 J/m for S1, a material composed only of epoxy resin, indicates its inadequate capacity to absorb and dissipate impacts. As the composition alters, the impact strength progressively increases.

Table 2. Comparative mechanical properties of hybrid composites (Relative to S1)

Sample	Tensile Strength (MPa) Change vs. S1	Tensile Modulus (GPa) Change vs. S1	Flexural Strength (MPa Change vs. S1	Flexural Modulus (GPa) Change vs. S1	Impact Strength (J/m) Change vs. S1
S1	23.13	2.83	47.22	2.62	2.12
S2	+83%	+59%	+65%	+83%	+150%
S3	+181%	+147%	+116%	+186%	+268%
S4	+211%	+225%	+144%	+274%	+306%
S5	+239%	+261%	+172%	+320%	+344%
S6	+311%	+338%	+199%	+388%	+475%
S7	+476%	+432%	+309%	+611%	+814%

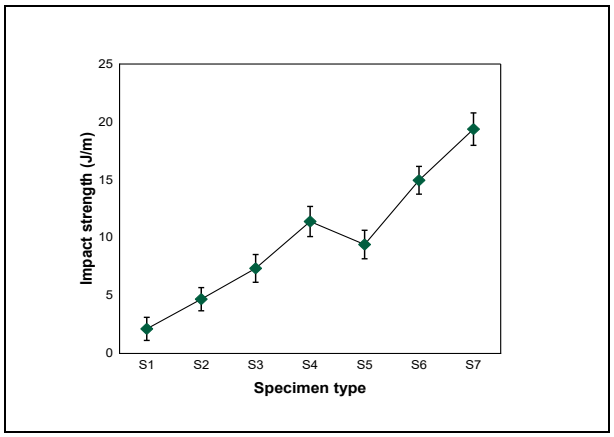


Fig. 7: Impact strength of the hybrid composites

The samples S2–S5 exhibit a maximum energy of 9.41 J/m in S5. The superior energy absorption and shock-absorbing characteristics of natural fibers significantly contribute to this enhancement, alleviating the effects of sudden loads. The use of ZnO nanoparticles and areca sheath powder enhances matrix reinforcement, hence augmenting impact strength by establishing additional barriers to fracture propagation.

Sample S7 attains a peak impact strength of 19.37 J/m. This indicates that the material endures elevated stress levels due to the incorporation of fillers and reinforcing fibers. Reinforcements and fillers significantly affect impact resistance, demonstrated by an average increase of around 513.7% in impact strength across samples relative to S1. The results indicate that the integration of natural fibers and fillers enhances impact resistance and synergistically improves energy absorption capabilities.

3.3 Microstructural Analysis

The SEM images of the tensile-fractured surfaces of bamboo fiber (20 wt%) reinforced epoxy composites containing 1wt% ZnO nanoparticles depict the fracture morphology and failure mechanisms comprehensively. The images collectively illustrate fiber rupture, fiber extraction, matrix failure, void creation, nanoparticle distribution, and river patterns, which are indicative of the tensile fracture response in natural fiber-reinforced composites. Fig. 8 (a) clearly depicts both fiber pull-out and fiber fracture, along with neighboring voids, indicating a mixed failure mode (S2). The fiber pull-out demonstrates localized weak adhesion between the fiber and matrix, caused by insufficient resin wetting or entrapped air during manufacturing, leading to inadequate load transfer. The existence of fractured fibers signifies that, in certain regions, the applied force was effectively conveyed from the epoxy matrix to the bamboo fibers, resulting in their failure. Fig. 8(b) depicts voids linked to matrix failure, where insufficient resin infiltration and localized stress concentrations enabled fracture initiation and propagation, hence reducing the total tensile strength (S3).

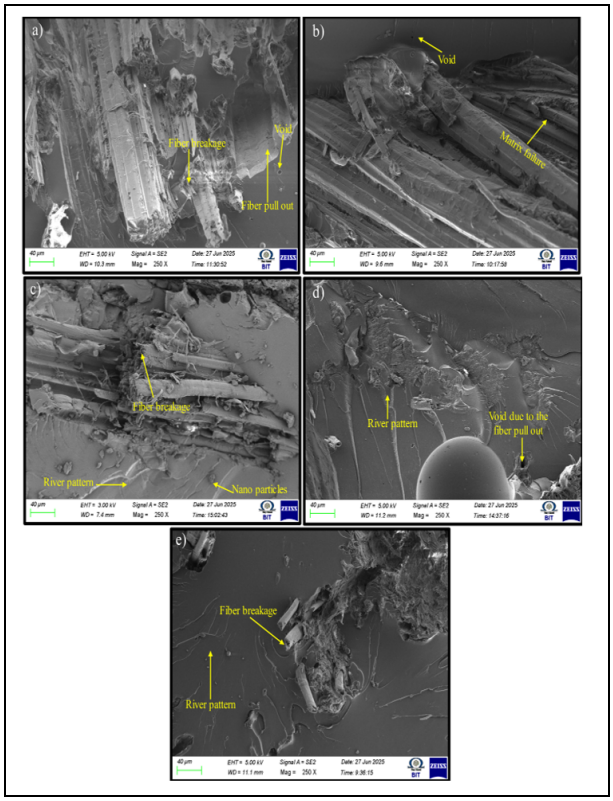


Fig. 8: Microstructural analysis of bamboo/*Sansevieria cylindrica*/areca sheath powder/ZnO-based hybrid composites

In Fig. 8(c), fiber fracture predominates, accompanied by river patterns and distributed ZnO nanoparticles (S4). The nanoparticles augment interfacial adhesion by enhancing surface roughness and facilitating mechanical interlocking, compelling the fibers to fracture rather than being extracted. The river patterns signify the trajectory of crack propagation inside the epoxy matrix, a characteristic indicator of brittle failure; however, the interplay of fibers and nanoparticles diverted the cracks, absorbing extra energy. Fig. 8(d) illustrates voids resulting from fiber pull-out, accompanied by distinct

river patterns, indicating that fracture propagation was affected by both weak interfacial areas and robust fiber–matrix bonding regions (S5). These voids, while harmful, offer significant insights regarding areas of stress concentration and the necessity of optimizing processing. Fig. 8(e) illustrates significant fiber breaking characterized by different river patterns, affirming that well-bonded bamboo fibers played a crucial role in resisting tensile loads, leading to fracture instead of debonding (S6). The hybrid composite shows fiber pull-out, void formation, and rough fractured surfaces, indicating interfacial debonding. The presence of ZnO nanoparticles and areca sheath powder improves adhesion and load transfer, reducing delamination (S7).

3.4 Dynamic Mechanical Analysis

3.4.1 Storage Modulus

The energy retained in the elastic structure of a material is indicated by its storage modulus (E′), which quantifies the material's elastic responses (Chen *et al.* 2022). The assessment of stiffness and elasticity in composites is essential. Fig. 9 illustrates the variation of the storage modulus of the manufactured materials as a function of temperature. The storage modulus graph distinctly indicates that the fiber-reinforced composite (S2), comprising 20wt% bamboo fiber and *Sansevieria cylindrica*, surpassed the simple epoxy (S1) composite regarding storage modulus values. The storage modulus of the S2 composite increased markedly from 1780 MPa (S1) to 2000 MPa within the 80-120 °C range, a region around the transitional temperatures. The S4 hybrid composite, containing 2wt% ZnO nanoparticles, exhibited an enhanced storage modulus of 1950 MPa following hybridization with natural fibers, areca sheath powder (S5 and S6), and ZnO (S3 and S4). The storage modulus of S7 composite (2150 MPa) exceeded that of S3 (1950 MPa) and S5 (2150 MPa) composites. Due to its elevated storage modulus, ZnO nanoparticles contribute to the improved elastic properties observed in hybrid composites, particularly in S4. Fig. 9 indicates that the storage moduli of the S3 and S4 composites exceed those of S5 and S6, hence supporting these conclusions.

The favorable impact of the hybrid effect on elasticity intensifies with a substantial presence of ZnO nanoparticles in the hybrid composite, enhancing stress transfer among the epoxy matrix and the natural fibers. The improved performance results from the rigidity of ZnO nanoparticles and their extensive surface area, facilitating improved load transmission and matrix interaction. A comparable effect of ZnO is noted when areca sheath powder is incorporated into S5 and S6 at concentrations of 1 wt% and 2wt%, respectively, enhancing the storage modulus, albeit to a lesser degree. Despite the easier dispersion of ZnO nanoparticles, the intrinsic characteristics of areca sheath powder render them a superior option for enhancing stiffness. The composite elasticity progressively diminished following the addition of areca sheath powder. Areca sheath powder surpasses all other composites in storage modulus (2220 MPa) when compared to the hybrid (S3-S6-type) composites. This illustrates a synergistic effect, wherein the augmented stiffness results from the collaboration of both reinforcements. The storage modulus values of composites decreased to a minimum and thereafter stabilized when the temperature was above 90 °C, indicating the matrix attained a rubbery condition.

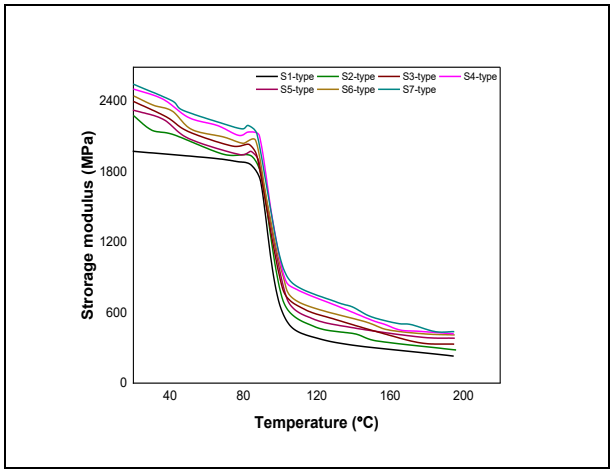


Fig. 9: Storage modulus of bamboo/*Sansevieria cylindrica*/areca sheath powder/ZnO-based hybrid composites

3.4.2 Loss Modulus

In contrast to the storage modulus, the loss modulus (E) serves as a metric for assessing the viscosity of a polymer. The amount of heat emitted due to energy dissipation during cyclic loading is utilized to examine this variable. Fig. 10 depicts the hybridized reinforcement polymeric composites and loss modulus curves of epoxy across a temperature spectrum of 200 °C. The loss modulus curve is uniform across all composites. In the transition zone, ranging from 80 to 120 °C, a linear increase occurs. At lower temperatures, a gradual increase occurs, while at higher temperatures, a rapid decrease transpires. The apex of the loss modulus curve serves as a reliable indicator of the glass transition temperature (T_g). In the absence of fiber reinforcement, the molecular bonds in the epoxy exhibit increased flexibility, evidenced by the clean epoxy's lowest loss modulus peak at 59 MPa. S7 exhibited a loss modulus of 120 MPa, whereas S6 had a loss modulus of 105 MPa.

The elevated peak ratings for both composites indicate their enhanced capacity to bond fibers to the matrix compared to the other composites, particularly S7. The two materials exhibited greater ZnO nanoparticles loadings than the other composites, suggesting that the ZnO nanoparticles reinforcements enhance the viscosity

properties. Energy is more effectively dissipated by nanoparticles owing to their larger surface area and interactions with a polymer matrix. The loss modulus significantly increases when natural fibers and areca sheath powder are hybridized at weight percentages of 20wt% and 2wt%, respectively. S4 (95 MPa) and S5 (98 MPa) hybrid composites had marginally lower loss modulus peaks in comparison to S7. The elevation of the peak to a higher temperature range, without concomitant enhancements in viscous performance, indicates that increasing matrix concentration of areca sheath powder filler has enhanced the thermal stability of the composites. The diminished mobility of the polymeric link segments, attributed to the reinforced fiber, accounts for the enhanced thermal stability.

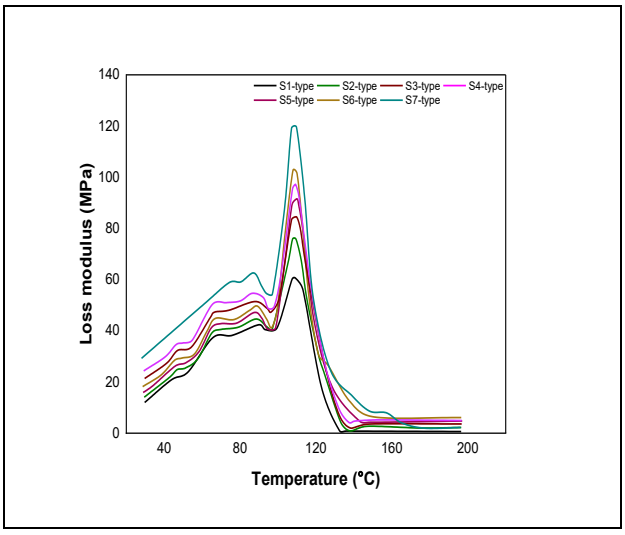


Fig. 10: Loss modulus of bamboo/*Sansevieria cylindrica*/areca sheath powder/ZnO-based hybrid composites

3.4.3 Damping Factor

The damping factor, referred to as the ratio of the loss modulus to the storage modulus or tan δ, illustrates the influence of viscosity, resistance, and elasticity on a material's behavior. A high tan δ value shows a viscous material with improved energy dissipation capabilities, while a low δ value is with a highly elastic material that retains energy inside its crystalline structure. Fig. 11 illustrates the tan δ values of epoxy composites reinforced with hybrid fibers within a temperature range of 20-200 °C. The maximum values of the storage modulus, loss modulus, tan δ, and T_g are presented in Table 3, calculated from the corresponding curves.

Fig. 11 illustrates that S1 had the lowest tan δ peak, indicating low viscosity and restricted mobility of polymer chains. The incorporation of fillers into the matrices significantly influences the damping characteristics of the composites, resulting transition from a viscoelastic material to an elastic one relative to the unmodified matrix, as evidenced by the improved tan δ peaks. Composite S7 showed the most substantial enhancement in tan δ, rising from 0.041 to 0.056, a 32% increase in reinforced materials. S4 composite exhibited a 25% enhancement in tan δ peak compared to that of S1. The composite exhibits increased flexibility due to the reinforcing ZnO nanoparticles, which have improved chain mobility and enhanced adhesion at the fiber-matrix interfaces. S5 and S6 exhibited comparable reduction in tan δ. The results indicate that the damping performance of the composite is unchanged by the hybrid addition of areca sheath powder filler.

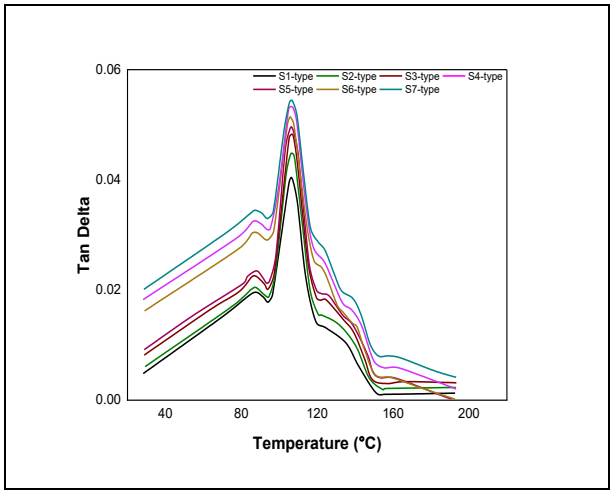


Fig. 11: Damping factor of fax/*Sansevieria cylindrica*/areca sheath powder/ZnO-based hybrid composites

Table 3. Glass transition temperature of bamboo fiber/*Sansevieria cylindrica*/areca sheath powder/ SiO_2-based composites

Sample	Storage Modulus Peak Height	Peak Height	Loss Modulus Peak Height	Tem (°C)	
	(MPa)	tan δ	(MPa)	Tg from Loss Modulus	Tg from tan δ
S1	1780	0.041	59	70.12	55
S2	1950	0.043	120	74.4	58.33
S3	2050	0.045	105	78.14	61.67
S4	2150	0.048	95	81	66.67
S5	1950	0.051	98	82.3	71.67
S6	2150	0.053	103	84.01	75
S7	2220	0.056	114	86.32	78.12

The tan δ plot indicated an increase in T_g from 55 to 80 °C, suggesting that the incorporation of natural fiber marginally enhanced thermal stability. Compared to S7, S2 showed higher T_g values. Likewise, compared to S5 and S6 composites, S3 and S4 also demonstrated the highest glass transition temperature. This finding

indicates that, relative to areca sheath powder, ZnO nanoparticles markedly improve the thermal stability of the composites. The composite exhibits enhanced molecular chain crosslinking because of its superior thermal stability. The T_g values obtained from the loss modulus peaks exhibited a comparable pattern. The hybrids exhibited T_g values ranging from 82.8 to 84.4 °C. The trend indicated by the loss modulus data seems more reliable in comparison to the T_g values obtained using both approaches. Yet all reinforced fillers exhibited improved thermal stability. Regarding thermal stability, composites composed of natural fibers showed the greatest and least enhancement, whereas hybrid materials demonstrated a moderate improvement. Comprehensive studies on hybrid reinforced composites have confirmed the reliability and precision of T_g data derived from the loss modulus.

3.5 Fire-retardant Properties

Fig. 12 shows the results of all the composite samples, facilitating a comprehensive assessment of the flammability characteristics. Heat release rate (HRR), effective heat of combustion (EHC), total heat release, mass loss rate (MLR), specific extinction area (SEA), yield of carbon monoxide (YCO), yield of carbon dioxide (YCO_2), time to ignition (TTI), and total smoke release (TSR) are hypothetical flammability characteristics for each composite (S1-S7). S7 showed the most pronounced enhancement in flame retardancy. Composites exhibiting this characteristic should provide enhanced flame resistance due to their reduced HRR (104.05 kW/m^2). These fillers diminished the overall combustible content of the composites, leading to a lower EHC (12.7 MJ/kg). The flammability characteristics of the composite materials are calculated using equations (1-8).

$$\mathrm{HRR} = \frac{\Delta Q}{\Delta t} \quad \ldots (1),$$

where Δt denotes the time interval and ΔQ signifies the rate of heat emission during combustion.

$$\mathrm{THR} = \int_{t_1}^{t_2} \mathrm{HRR}(t)dt \quad \ldots (2)$$

when the combustion initiates and concludes at intervals t_1 and t_2, respectively

$$\mathrm{EHC} = \frac{\mathrm{THR}}{m} \quad \ldots (3)$$

The material mass is denoted by m.

$$\mathrm{MLR} = \frac{\Delta m}{\Delta t} \quad \ldots (4),$$

where Δb denotes the time interval and m signifies mass loss.

$$\mathrm{TTI} = t_{\mathrm{ignition}} - t_{\mathrm{start}} \quad \ldots (5)$$

$$\mathrm{SEA} = \frac{A}{m} \quad \ldots (6)$$

The material mass is denoted by b, whereas A signifies the area under the smoke generation curve.

$$\mathrm{TSR} = \int_{t_1}^{t_2} \text{Smoke production } (t)dt \quad \ldots (7)$$

$$\mathrm{YCO \text{ or } YCO_2} = \frac{m_{\mathrm{CO}}}{m_{\mathrm{total}}} \text{ or } \frac{m_{\mathrm{CO_2}}}{m_{\mathrm{total}}} \quad \ldots (8)$$

The formula considers the initial and final times of the smoke, the masses of carbon monoxide and carbon dioxide, and the total mass of combustion gas, referred to as m_{total}.

Table 4 displays the fire-retardant properties of the hybrid composites. The superior flame-retardant capabilities of S7 are further emphasized by the decreasing trends in THR(183.39 MJ/m²) and MLR (0.025 g/s) with increased filler content. Filler materials absorb and dissipate heat in contrasting manners, hence reducing THR and MLR, respectively. S7 composite, due to its reduced THR and slower combustion rate, maintains its structural integrity for an extended duration during combustion relative to other composites. In an earlier study, epoxy/flax–cotton composites with APP and vermiculite (1–10 wt%) were studied. Small vermiculite additions (1–2 wt%) yielded synergistic flame-retardant effects, reducing HRR by 60% and THR by 20%, while maintaining acceptable mechanical properties. Higher filler levels weakened the composite structure (Barczewski *et al.* 2023).

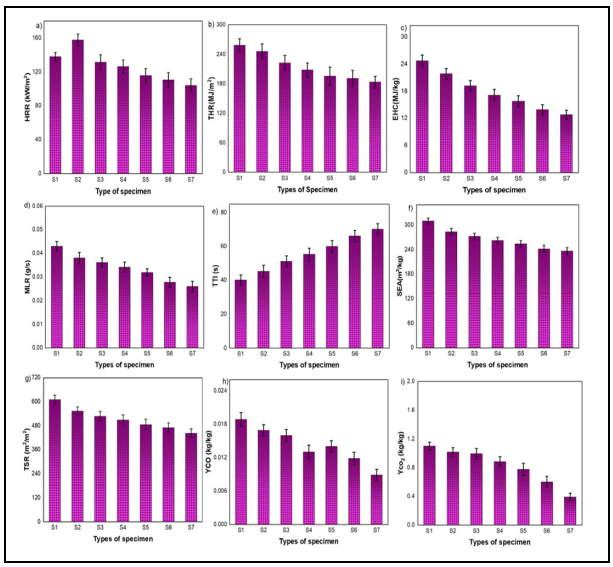


Fig. 12: Fire-retardant performance of hybrid composites, showing (a) heat release rate, (b) total heat release, (c) effective heat of combustion, (d) mass loss rate, (e) time to ignition, (f) specific extinction area, (g) total smoke release, (h) carbon monoxide emission and (i) carbon dioxide emission

The SEA (236.53 m^2/kg) quantifies the reduction in smoke production attributable to the incorporation of these fillers. S7 is safer for use in smoke suppression-critical regions, as fillers assist in the combustion of smoke from incomplete burning. The YCO and YCO_2 are essential measures for assessing combustion efficiency. The S7 composite demonstrates the lowest YCO and minimal gas toxicity due to incomplete combustion, resulting in the highest YCO_2. This phenomenon occurs due to accelerated combustion rates of the fillers. The TTI (72s), a significant performance indicator, is elevated for S7 composite, showing its superior resistance to ignition. The fillers enhance inertial forces of blends, rendering them less flammable and delaying fire onset. Moreover, S7 has the lowest TSR at 442.50 m^2/ m^2, indicating minimal smoke emission during combustion, a critical factor for visibility and safety in fire scenarios.

Table 4. Flammability characteristics of bamboo fiber/*Sansevieria cylindrica* fiber/areca sheath powder/ SiO_2-based hybrid composites

Symbol	THR (MJ/m^2)	HRR (kW/m^2)	MLR (g/s)	EHC (MJ/kg)	SEA (m^2/kg)	TTI (s)	Y_{CO} (kg/kg)	TSR (m^2/m^2)	Y_{CO2} (kg/kg)
S1	258.29	137.91915	0.04	24.7	310.5	40	0.01	611.3	1.10
S2	246.042	157.72843	0.03	21.83	284.2	45.3	0.016	553	1.015
S3	222.54	131.4	0.036	19.17	272.6	51.1	0.015	527.9	0.99
S4	208.25	126.25	0.034	17.15	262.5	55.2	0.013	509.3	0.88
S5	195.9	115.77	0.031	15.81465	254.3	59.9	0.0140	486	0.77
S6	191.0	110.66	0.02	13.9	242	66.2	0.011	470.5	0.60
S7	183.3	104.0	0.025	12.79	236.5	70.2	0.0089	442.5	0.39

The synergistic usage of areca sheath powder, ZnO nanoparticles, and natural fibers gives S7 an advantage in flammability performance. The flammability is enhanced in multiple ways by this combination. By layering non-combustible areca sheath powder and ZnO nanoparticles—which, when combined with natural fibers, reduce HRR, limit flame spread, and dissipate heat—it creates a thermal barrier effect that inhibits burning. In addition, the use of ZnO and areca sheath powder has decreased the composite's combustible content, which improves structural stability, increases resistance to heating effects, and decreases both the EHC and THR. Finally, the use of ZnO and areca sheath powder materials improves the efficiency of reactions involving full combustion. These materials increase heat transfer rates, CO_2 yield, and oxygen diffusion, all of which contribute to a decrease in the production of harmful gases. Once again, the composite has extremely low SEA and TSR, meaning it smokes very little; as a result, fire situations involving it are much easier to manage. A greater TTI and a noticeable resistance to both heat transfer and ignition are indicators that S7 exhibits a retardancy to ignition.

3.6 Vibration Results

Three vibrational modes in S3-to-S7 hybrid composites were investigated. Deformation of the hybrid composites was accomplished by exerting a steady stress on a cantilever structure across five specific locations utilizing a piezoelectric impact hammer. The study sought to ascertain the frequency and damping values associated with composite beams with three deformation modes of secondary bending, bending and twisting. Three unique modes were employed for the vibration analysis, bending, twisting, and secondary bending. This experimental design and analysis are crucial for applications requiring vibration control and damping, as they illustrate the effect of including ZnO and Areca sheath powder on the damping properties of composite materials.

3.7 Natural Frequency of Hybrid Composites

Fig. 13 illustrates natural frequency data, indicating increase in nanofiller inside hybrid composite materials leads to progressive elevation of natural frequency.

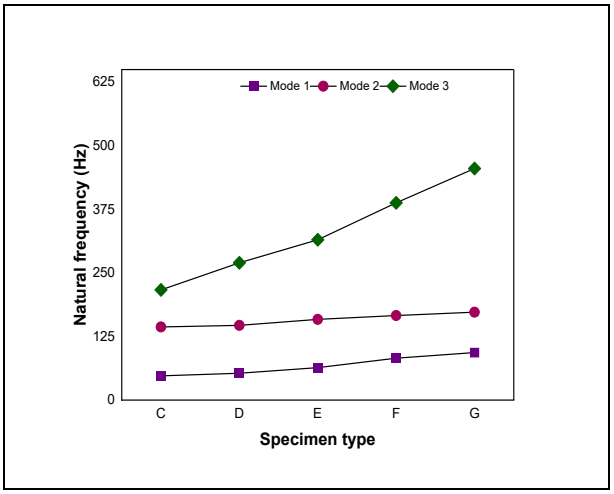


Fig. 13: Frequency response behavior of hybrid composites across three modes

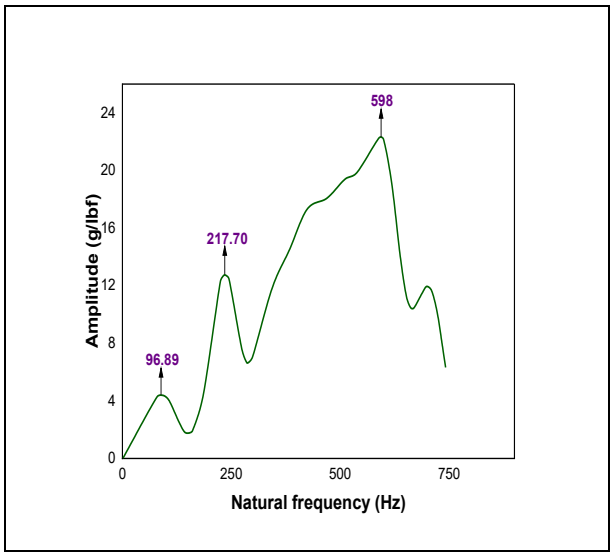


Fig. 14: Frequency response characteristics of S7

Specimen S7 consistently exhibits the highest natural frequencies across all modes, indicating dynamic characteristics. S7 has a natural frequency of 96.89 Hz, whereas specimen S3 displays a frequency of 55 Hz. Specimen S7 attains a natural frequency of up to 217.70 Hz, but specimen S3 is limited to a maximum frequency of 162 Hz. The results indicate that the use of nanofillers in composites progressively enhances modal frequencies.

Various scientific factors have led to the rising natural frequencies in S7. The incorporation of nanofillers, specifically ZnO nanoparticles and areca sheath powder has markedly improved the stiffness and rigidity of the composite matrix. The natural frequencies employed in this study were elevated due to the diminished vibrational amplitude and increased structural resonance frequency resulting from the augmented stiffness. The interfacial bonding among the matrix and nanofillers facilitates more effective stress transfer between phases, hence enhancing the dynamic characteristics of S7 composite by reducing energy losses due to vibration. In summary, S7 composite is ideal for applications necessitating controlled vibrations and enhanced structural stability due to their heightened stiffness, improved stress transfer, and optimized reinforcement mechanisms, which collectively yield an exceptional response concerning natural frequency. Fig. 14 depicts the frequency response of S7.

4. CONCLUSION

The study on composites reinforced with *Sansevieria cylindrica*/bamboo fibers, ZnO nanoparticles, and areca sheath powder showed major improvements in mechanical, thermal, and dynamic properties. FTIR confirmed hybridization through hydroxyl (–OH) and Si–O groups. Mechanical testing revealed large gains: tensile strength rose from 23.13 MPa (S1) to 133.11 MPa (S7), tensile modulus from 2.83 to 15.07 GPa, and flexural strength/modulus from 47.22 MPa & 2.62 GPa to 192.97 MPa & 18.65 GPa. Impact strength improved from 2.62 to 19.37 J/m. Dynamic mechanical analysis showed that ZnO nanoparticles enhanced elasticity and load transfer due to high stiffness and surface area, while areca sheath powder contributed to stiffness at lower levels. Fire-retardant properties were highest in S7 composite, with reduced heat release and emissions. Vibration analysis showed maximum natural frequency (96.89 Hz), highlighting superior energy dissipation and stability. Thus, S7 demonstrated high strength, durability, and dynamic stability. Potential applications include lightweight aircraft panels, automotive body and chassis components, and marine structures due to their mechanical strength, vibration damping, and resistance to moisture and corrosion.

FUNDING

This research received no specific grant from any funding agency in the public, commercial, or not-for-profit sectors.

CONFLICTS OF INTEREST

The authors declare that there is no conflict of interest.

COPYRIGHT

This article is an open-access article distributed under the terms and conditions of the Creative Commons Attribution (CC BY) license (http://creativecommons.org/licenses/by/4.0/).

REFERENCES

Al-Lhaibi, S. A. and Al-Shabander, B. M., Study the effect of ZnO nanoparticles reinforced sawdust /epoxy composites on mechanical properties, *Dig. J. Nanomater. Biostruct.*, 17(3), 851–860(2022). https://doi.org/10.15251/DJNB.2022.173.851

Barczewski, M., Sałasińska, K., Raś, W., Hejna, A., Michałowski, S., Kosmela, P., Aniśko, J., Boczkowska, A. and Szostak, M., The effect of hybridization of fire retarded epoxy/flax-cotton fiber laminates by expanded vermiculite: Structure-property relationship study, *Adv. Ind. Eng. Polym. Res.,* 6(2), 181–194(2023). https://doi.org/10.1016/j.aiepr.2023.01.005

Chen, J., Gu, S., Li, W., Yuan, Z. and Cheng, H., Effects of NaOH alkali treatment concentration on the properties of moso bamboo strips and their epoxy resin composites, *Nongye Gongcheng Xuebao/ Trans. Chin. Soc. Agric. Eng.*, 38(15), 234–240(2022). https://doi.org/10.11975/j.issn.1002-6819.2022.15.025

Diharjo, K., Gapsari, F., Andoko, A., Wijaya, M. N., Mavinkere Rangappa, S. and Siengchin, S., Flammability and thermal resistance of Ceiba petandra fiber-reinforced composite with snail powder filler*, Polym. Compos*., 45(6), 4947–4960 (2024). https://doi.org/10.1002/pc.28100

Giridharan, K., Sasirekha, S., Padmanabhan, S., Chakravarthi, G. and Stalin, B., Effect of green pea pod lignin addition on thermal degradation, flame resistance, DMA, and creep resistance of pineapple fibre epoxy composite, *Biomass Convers. Biorefin.*, 14(23), 29843–29852(2024). https://doi.org/10.1007/s13399-023-04841-2

Gupta, R. K., Mayakannan, S., Vijayaraghavalu, S., Poornima, M. M., Nanthakumar, S. and Bhaskaran, N. A., Multi-objective Optimization of Bamboo-madar Fiber Reinforced Composites for Lightweight Automotive Applications using Machine Learning and Genetic Algorithms, *J. Environ. Nanotechnol*., 13(4), 358–376(2024). https://doi.org/10.13074/jent.2024.12.244978

Harak, S. S., Krishnaveni, K., Karthick, K., Chinnarasu, K., Prasad, V. H. P., Tonk, A. and Mayakannan, S., Experimental Study on the Mechanical Properties of Hybrid Areca and Abaca Fiber Reinforced Polymer Composites*, J. Environ. Nanotechnol*., 13(4), 92–101(2024). https://doi.org/10.13074/jent.2024.12.244977

Iyyadurai, J., Arockiasamy, F. S., Manickam, T., Rajaram, S., Suyambulingam, I. and Siengchin, S., Experimental Investigation on Mechanical, Thermal, Viscoelastic, Water Absorption, and Biodegradability Behavior of Sansevieria Ehrenbergii Fiber Reinforced Novel Polymeric Composite with the Addition of Coconut Shell Ash Powder, *J. Inorg. Organomet. Polym. Mater.,* 33(3), 796–809(2023). https://doi.org/10.1007/s10904-023-02537-8

Khan, M. K. A., Faisal, M. and Prakash, V. R. A., Effect of silane coupling grafted polyethylene terephthalate foam and areca fruit fiber reinforced chitin modified vinyl ester prosthetic composite on thermal and water accelerated aging conditions, *Polym. Compos*., 45(6), 5111–5124(2024a). https://doi.org/10.1002/pc.28114

Khan, M. K. A., Faisal, M. and Prakash, V. R. A., Characterization of sea urchin spike chitin macromolecule and basalt-encapsulated bamboo fiber-epoxy environmental friendly composite for human prosthetic application, *Polym. Bull.,* 81(12), 10767–10785(2024b). https://doi.org/10.1007/s00289-024-05208-x

Krishnasamy, B., Thirugapillai, P., Rajakannu, A. and Selvaraju, M., Optimization and multi-objective analysis of tensile, flexural and impact strength in nano-hybrid bio-composites reinforced with Helicteres isora, Holoptelea integrifolia fibers, and nanographene, *Revista Materia*, 30, 240864(2025). https://doi.org/10.1590/1517-7076-RMAT-2024-0864

Kumar, R. and Chauhan, S., Effect of ammonium polyphosphate as synergist with nano silica dioxide on flammability of boron compound pretreated bamboo flour-HDPE composite, *Fire Saf. J.,* 133, 103647(2022). https://doi.org/10.1016/j.firesaf.2022.103647

Kumar, R., Gunjal, J. and Chauhan, S., Effect of borax-boric acid and ammonium polyphosphate on flame retardancy of natural fiber polyethylene composites, *Maderas: Ciencia y Tecnologia*, 24, 1-10(2022). http://dx.doi.org/10.4067/s0718-221x2022000100434

Lan, X., Bian, C., Yang, Y., Zhang, Q. and Huang, G., Modified Epoxy Resin on the Burning Behavior and Mechanical Properties of Aramid Fiber, *Compos. Mater*, 17(16), 4028(2024). https://doi.org/10.3390/ma17164028

Li, W., Zhang, L., Chai, W., Yin, N., Semple, K., Li, L., Zhang, W. and Dai, C., Enhancement of flame retardancy and mechanical properties of polylactic acid with a biodegradable fire-retardant filler system based on bamboo charcoal, *Polym.*, 13(13), 2167(2021). https://doi.org/10.3390/polym13132167

Manickaraj, K., Ramamoorthi, R., Sathish, S. and Makeshkumar, M., Effect of hybridization of novel African teff and snake grass fibers reinforced epoxy composites with bio castor seed shell filler: Experimental investigation, *Polym. Polym. Compos.,* 30, 2288(2022). https://doi.org/10.1177/09673911221102288

Narayanan, L. and Muthukumaran, S., Development of silane-treated corn husk fiber and agro-waste biofiller-reinforced epoxy composite: effects on wear, mechanical, thermal, and water absorption properties, *Biomass Convers. Biorefin.*, 14(23), 30801–30817 (2024). https://doi.org/10.1007/s13399-024-05837-2

Ngouobe, J. N., Lecompte, T., Ngohe-Ekam, P. S., Nfornkah, B. N., Bailleul, J. L., Kervoelen, A., Magueresse, A., Bastianelli, F., Noah, P. M. A., Kanmogne, A., Bayeck, A. J. P. and Szczepaniak, R., Comparative study of the physical and mechanical properties of Bambusa vulgaris fibers from Cameroon for application to hybrid composite materials, *Ind. Crops Prod.,* 222(3), 119725(2024). https://doi.org/10.1016/j.indcrop.2024.119725

Pachiappan, A. and Santhanam, S. K. V., Mechanical behavior of snake grass fiber with neem gum filler hybrid composite, *Polimeros*, 33(3), 0033(2023). https://doi.org/10.1590/0104-1428.20220116

Palanisamy, S., Kalimuthu, M., Dharmalingam, S., Alavudeen, A., Nagarajan, R., Ismail, S. O., Siengchin, S., Mohammad, F. and Al-Lohedan, H. A., Effects of fiber loadings and lengths on mechanical properties of *Sansevieria cylindrica* fiber reinforced natural rubber biocomposites, *Mater. Res. Exp.,* 10(8), 85503(2023). https://doi.org/10.1088/2053-1591/acefb0

Ponnuswamy, M., Sathishkumar, T. P., Selvaraju, M. and Sundramurthy, V. P., Enset ventricosum Fibre-Based Biocomposite Preparation with Wood Apple Shell Particles as a Filler: Effect of Alkali Treatment and Optimization of Composition for Physio-Mechanical Properties, *Arabian J. Sci. Eng.,* 49(11), 15733–15748(2024). https://doi.org/10.1007/s13369-024-09253-6

Prabhu, P., Karthikeyan, B., Ravi, R. M. V. R. and Balaji, A., Investigation on mechanical, dynamic mechanical analysis, thermal conductivity, morphological analysis, and biodegradability properties of hybrid fiber mats reinforced HLCE resin nanocomposites, *Polym. Compos*., 43(12), 8850–8859(2022). https://doi.org/10.1002/pc.27066

Raja, T. and Devarajan, Y., A novel way of converting waste-enriched composites to lightweight, biodegradable resources: a property analysis, *Biomass Convers. Biorefin.,* 14(16), 19431–19441(2024). https://doi.org/10.1007/s13399-023-03872-z

Raja, T., Devarajan, Y., Patel, G. M., Nath, J. K., Kalidhas, A. M., Sharma, S. and Chaudhary, P., Sustainable enhancement of Henequen fiber-reinforced polymer composites with copper oxide nanoparticles: A step forward in clean engineering and technology, *Cleaner Eng. Technol.*, 27, 101039(2025). https://doi.org/10.1016/j.clet.2025.101039

Ramadoss, P. K., Mayakrishnan, M. and Arockiasamy, F. S., Discarded custard apple seed powder waste-based polymer composites: an experimental study on mechanical, acoustic, thermal and moisture properties, *Iran. Polym. J.,* 33(4), 461–479(2024). https://doi.org/10.1007/s13726-023-01266-6

Saha, A., Kulkarni, N. D., Kumar, M. and Kumari, P. (2024). The structural, dielectric, and dynamic properties of NaOH-treated Bambusa tulda reinforced biocomposites—an experimental investigation, *Biomass Convers. Biorefin.,* 14(20), 26247–26266(2024). https://doi.org/10.1007/s13399-023-04709-5

Sasaki, S., Naito, K. and Uchidate, M. Development of polylactic acid-untreated bamboo filler composite and its chemical and mechanical properties, *J. Appl. Polym. Sci.,* 141(23), 55461(2024). https://doi.org/10.1002/app.55461

Sathish, K. R., Vandhana, D. V., Nivedhitha, D. M., Srish, S. S., Visakan, S., Bharath, S. S. and Sathish, K. S. B. Effect of nanoparticles in natural fiber reinforced polymer composites, *Mater. Today: Proc*., 20266(2023). https://doi.org/10.1016/j.matpr.2023.04.130

Singh, S., Singh, A. and Sharma, S. K. Analytical Prediction Models for Density, Thermal Conductivity and Mechanical Strength of Micro-scaled Areca Nut Powder-Reinforced Epoxy Composites, *J. Inst. Eng. India Ser. C*, 101(1), 43–51(2020). https://doi.org/10.1007/s40032-019-00535-9

Subramaniam, B., Manickavasagam, V. M., Rajakumar I, P. T., Raj, P. A. C., Bharath, V. G., Madhusudhanan, J., Sharma, A. K., Patil, P. and Assefa, G. B., Investigation of Mechanical Properties of *Sansevieria cylindrica* Fiber/Polyester Composites, *Adv. Mater. Sci. Eng.*, 6(1), 2180614(2022). https://doi.org/10.1155/2022/2180614

Torres, M., Rodriguez, V. R., Alcantara, P. I. and Franco-Urquiza, E., Mechanical properties and fracture behaviour of agave fibers bio-based epoxy laminates reinforced with zinc oxide, *J. Ind. Text.*, 51(4), 5847S-5868S(2022). https://doi.org/10.1177/1528083720965689

Velmurugan, G., Chohan, J. S., Kumar, G., Shankar, V. S. and Nagaraj, M., Innovative building thermal insulation: bamboo fiber-based eco-composite with eggshell powder and cardboard waste reinforcement, *J. Balkan Tribol. Assoc.,* 31(3), 388–408(2025).

Velmurugan, G., Babu., K., Nagaraj, M. and Kumar, A. J. P., Investigations of Flame Retardancy, Mechanical and Thermal Properties of Woven Hemp/PP Hybrid Composite for Insulating Material Reinforced with Synthetic Silicon and Zinc Oxides, *Silicon*, 15(11), 4875–4888(2023). https://doi.org/10.1007/s12633-023-02408-4